Published in final edited form as:
Dev Cell. 2011 May 17; 20(5): 583–596. doi:10.1016/j.devcel.2011.03.013.

The *WTX* Tumor Suppressor Regulates Mesenchymal Progenitor Cell Fate Specification

Annie Moisan[#1], **Miguel N. Rivera**[#1,2], **Sutada Lotinun**[5], **Sara Akhavanfard**[2], **Erik J. Coffman**[1,2], **Edward B. Cook**[1,2], **Svetlana Stoykova**[1], **Siddhartha Mukherjee**[4], **Jesse A. Schoonmaker**[3], **Alexa Burger**[1], **Woo Jae Kim**[1], **Henry M. Kronenberg**[4], **Roland Baron**[4,5], **Daniel A. Haber**[1,*], and **Nabeel Bardeesy**[1,*]

[1]Massachusetts General Hospital Cancer Center, Harvard Medical School, Boston, MA 02114, USA

[2]Department of Pathology, Harvard Medical School, Boston, MA 02114, USA

[3]Center for Regenerative Medicine, Harvard Medical School, Boston, MA 02114, USA

[4]Endocrine Unit, Harvard Medical School, Boston, MA 02114, USA

[5]Department of Oral Medicine, Infection and Immunity, Harvard School of Dental Medicine, Boston, MA 02115, USA

[#] These authors contributed equally to this work.

SUMMARY

WTX is an X-linked tumor suppressor targeted by somatic mutations in Wilms tumor, a pediatric kidney cancer, and by germline inactivation in osteopathia striata with cranial sclerosis, a bone overgrowth syndrome. Here, we show that *Wtx* deletion in mice causes neonatal lethality, somatic overgrowth, and malformation of multiple mesenchyme-derived tissues, including bone, fat, kidney, heart, and spleen. Inactivation of *Wtx* at different developmental stages and in primary mesenchymal progenitor cells (MPCs) reveals that bone mass increase and adipose tissue deficiency are due to altered lineage fate decisions coupled with delayed terminal differentiation. Specification defects in MPCs result from aberrant β-catenin activation, whereas alternative pathways contribute to the subsequently delayed differentiation of lineage-restricted cells. Thus, *Wtx* is a regulator of MPC commitment and differentiation with stage-specific functions in inhibiting canonical Wnt signaling. Furthermore, the constellation of anomalies in *Wtx* null mice suggests that this tumor suppressor broadly regulates MPCs in multiple tissues.

[*]Correspondence: haber@helix.mgh.harvard.edu (D.A.H.), bardeesy.nabeel@mgh.harvard.edu (N.B.).

SUPPLEMENTAL INFORMATION

Supplemental Information includes Supplemental Experimental Procedures, Supplemental References, and eight figures and can be found with this article online at doi:10.1016/j.devcel.2011.03.013.

INTRODUCTION

WTX is a recently identified tumor suppressor gene that is targeted by somatic mutations in up to 30% of cases of Wilms tumor, the most common type of pediatric kidney cancer (Rivera et al., 2007). Wilms tumor arises from multipotent mesenchymal kidney precursors and retains a limited capacity to differentiate into structures that resemble embryonic kidney tissue and, occasionally, ectopic elements such as muscle, bone, and fat (Rivera and Haber, 2005). The location of *WTX* on the X chromosome is of particular interest for a tumor suppressor, because a single somatic mutation or deletion targeting the X allele in males or the active X allele in females is sufficient to ensure gene inactivation (Rivera et al., 2007). Germline inactivation of *WTX* causes OSCS syndrome, a developmental disorder characterized by macrocephaly and osteosclerosis in females, and a high incidence of embryonic lethality in males (Jenkins et al., 2009). In addition to severe bone abnormalities, affected males have a variable incidence of other phenotypes, including cardiac and genitourinary defects (Perdu et al., 2010). Of note, other Wilms tumor-associated genes are known to play important roles in organogenesis; the WT1 zinc finger transcription factor, which is inactivated in Wilms tumor, regulates the development of kidneys and other organs (Kreidberg et al., 1993; Rivera and Haber, 2005), and β-catenin, which undergoes activating mutations (Koesters et al., 1999), is a central regulator of self-renewal and differentiation pathways throughout development.

WTX belongs to a family of proteins (FAM123) that do not contain domains with significant homology to genes of known function. Protein shuttling between the plasma membrane, cytoplasm, and nucleus suggests that WTX may interact with several distinct cellular pathways in these compartments (Rivera et al., 2009). Cytoplasmic WTX physically associates with components of the β-catenin destruction complex and inhibits Wnt signaling by enhancing the degradation of β-catenin (Major et al., 2007). A role for WTX in mediating the association of APC with the plasma membrane has also been described (Grohmann et al., 2007). Nuclear WTX is localized to paraspeckles, subnuclear compartments implicated in transcription and RNA processing, and it binds to WT1, leading to coregulation of a target transcript (Rivera et al., 2009). The contribution of WTX to the regulation of these pathways in vivo is not known, and more broadly, the key developmental processes controlled by this tumor suppressor have yet to be defined.

To gain insight into the developmental pathways regulated by *Wtx*, we generated a conditional *Wtx* knockout mouse model. Global deletion of *Wtx* causes neonatal lethality and prominent defects in bone, fat, kidney, heart, and spleen, a series of tissues that are derived from mesenchymal progenitor cell (MPC) populations. Pronounced alterations in bone and fat development are due to a critical requirement for *Wtx* in both specifying lineage commitment decisions of MPCs and in controlling the later maturation of lineage-restricted cells. Wtx acts to suppress canonical Wnt signaling in early multipotent mesenchymal progenitors, whereas its subsequent role in lineage progression is mediated by alternate pathways. These observations identify Wtx as an important novel regulator of mesenchymal differentiation and a context-dependent β-catenin inhibitor, and provide a potential link between its role in normal tissue development and pediatric cancer.

RESULTS

Germline *Wtx* Knockout Causes Somatic Overgrowth and Developmental Defects in Multiple Tissues Derived from Embryonic Mesenchyme

To study *Wtx* function in vivo we generated a conditional knockout allele of *Wtx* (Wtx^{lox}) (see Figures S1A–S1F available online) and obtained heterozygous and homozygous mice by crosses to the *Gata1-Cre* general deleter strain (Figure S1G). All genotypes appeared grossly normal at embryonic day (E) 13.5, whereas at later stages of gestation *Wtx* null mice (male), and to a lesser extent *Wtx*-heterozygotes (female), exhibited increases in body size and mass compared to controls (Figures 1A, 1B, and S1I). *Wtx* null neonates became cyanotic and died within 24 hr of birth, whereas, most heterozygotes were viable and fertile (Figure S1H). Examination of *Wtx* null neonates revealed a set of abnormalities affecting the two organs implicated in *WTX*-related human diseases, kidneys, and bones, as well as heart, spleen, and adipose tissue (Figures 1 and S2). Dramatic overgrowth was observed in bone and heart, whereas spleen and adipose tissue were hypoplastic. The kidneys exhibited a complex phenotype consisting of either agenesis or over-growth, often within the same animal. Gross and histological analysis of other organs—including brain, lung, pancreas, liver, adrenals, and stomach—did not reveal additional abnormalities (Figure 1B and data not shown).

Notably, the tissues affected in *Wtx* null neonates share an origin in embryonic mesenchyme. In the kidney, a population of mesenchymal precursors known as the metanephric mesenchyme gives rise to most mature epithelia and is the likely origin of Wilms tumor. Kidney development is determined by interactions between the metanephric mesenchyme and the ureteric bud, an outgrowth of the Wolffian duct. Secreted signals from the metanephric mesenchyme induce the formation of the ureteric bud, which in turn invades the mesenchyme and triggers its differentiation into epithelial structures. Unilateral or bilateral renal agenesis was observed in 64% of *Wtx* null neonates (Figures 1C, left, and S2A)—a phenotype that has been associated with early mesenchymal dysfunction (Brodbeck and Englert, 2004) and that is consistent with the observed expression of *Wtx* in the metanephric mesenchyme and in early renal epithelial precursors (Rivera et al., 2007). In keeping with this pattern, immunostaining for cleaved caspase-3 at E13.5 revealed widespread apoptosis in the metanephric mesenchyme in a high proportion of *Wtx* null embryos (Figure S2C, top row, middle).

The early metanephric mesenchyme markers, Pax2 and Six2 (Brodbeck and Englert, 2004), were present diffusely in the uninduced *Wtx* null mesenchyme, indicating that there is initial specification of the metanephric mesenchyme but no condensation and epithelialization (Figure S2C and data not shown). Moreover, no ureteric bud-derived structures were detected and the Wolffian duct remained detached as shown by Pax2 staining, which also marks this structure (Figure S2C). In the subset of E13.5 *Wtx* null kidneys where ureteric bud branching was observed, the developing kidney structures showed normal histology and marker expression (Figure S2C, right). This pattern of unilateral agenesis is often observed in humans and animal models and is thought to result from a stochastic process, such that a signaling threshold required for ureteric bud recruitment is reached in one kidney but not in

the other, resulting in a grossly normal kidney matched with an absent contralateral organ (Brodbeck and Englert, 2004).

Neonatal mouse kidneys are not fully differentiated, but typically harbor persistent aggregates of proliferating precursor cells adjacent to the outer surface of the organ and expressing the renal stem cell marker, Six2 (Kobayashi et al., 2008). Remarkably, in contrast to cases of failed renal organogenesis, kidneys that did form in *Wtx* null neonates were significantly enlarged, and showed expansion of the $Six2^+$ mesenchymal progenitors and increased total *Six2* mRNA levels (Figures 1C, right, and S2D). Despite this stem cell expansion, the *Wtx* null neonatal kidneys showed no alterations in the staining pattern of Wt1— a marker of fully differentiated glomeruli at this time point (Pritchard-Jones et al., 1990)—indicating that mature epithelial structures were also present (Figure S2E). No differences in renal cell proliferation or apoptosis were observed in neonates (data not shown). Hence *Wtx* deficiency causes either renal agenesis or overgrowth, associated in both cases with alterations in the renal mesenchymal progenitors.

Bone and adipose tissue also arise from multipotent mesenchymal progenitors and both were affected by *Wtx* inactivation. Severe reductions in brown and white adipose tissue were observed in *Wtx* null neonates (Figures 1D and S2F). In addition, marked overgrowth and dysplasia of the skeleton was evident in *Wtx* null neonates, including enlargement of the cranial vault (Figure 1Ea), asymmetrical distribution of ossification centers along the sternum (Figure 1Eb), bowed radii and ulnas and malformed deltoid tuberosities (Figure 1Ec), and massive increases in mineralized matrix in cortical bone (Figure 1F). *Wtx* heterozygous neonates and adults also exhibited skeletal anomalies associated with increases in bone mineral density (Figures 1G, 1H, and S2G). These bone and adipocyte alterations raised the possibility that *Wtx* may affect the differentiation of early mesenchymal progenitors. Therefore, to define the functional consequences of *Wtx* inactivation in a well-characterized and accessible system, we focused on bone and adipocyte differentiation.

Wtx Ablation in Early Mesenchymal Progenitors Causes Aberrant Osteoblastogenesis Leading to Bone Overgrowth

Bone development is mediated by a balance between the activity of bone-forming osteoblasts, which arise from common mesenchymal progenitors to chondrocytes and adipocytes, versus bone-resorbing osteoclasts, which originate from hematopoietic progenitors (Boyle et al., 2003; Karsenty et al., 2009; Lefterova and Lazar, 2009; Rosen et al., 2009). To test the role of *Wtx* in the mesenchymal lineage, we employed the *Paired related homeobox 1-Cre* (*Prx1-Cre*) strain (Logan et al., 2002), which is active in mesenchymal progenitors of the long bones; the *Prx1* promoter has weak activity in the developing craniofacial mesenchyme precluding the use of this strain to study defects in the skull. *Prx1-Cre;*$Wtx^{lox/Y}$ mice were viable and showed full recapitulation of the *Wtx* null sternum and appendicular skeletal phenotype as neonates, along with accumulation of cortical and trabecular bone as adults (Figures 2A, 2B, and S3A). In marked contrast, *Wtx* ablation within committed chondrocyte precursors or within differentiated osteoblasts using the *Collagen2a1-Cre* (*Col2a1-Cre*) and *Osteocalcin-Cre* (*Ocn-Cre*) strains, respectively, did not result in gross differences in the neonatal or adult skeleton (Figures 2A and S3A) despite

effective Cre-mediated recombination (Figure S3F). Finally, use of *Osterix-Cre* (*Osx-Cre*) mice to delete *Wtx* in osteoblast precursors resulted in increased mineralization of the cortical and trabecular bone, although unlike the *Prx-Cre;Wtx*$^{lox/Y}$ mice, there was no evidence of increases in the width of the bones or of dysplasia (Figures S3B–S3D and data not shown). Thus, the bone defects caused by *Wtx* deficiency result from a requirement for *Wtx* function in multipotent MPCs and in early lineage-restricted precursors.

The role of *Wtx* in MPCs could involve cell autonomous effects on osteoblast number and/or activity, directly leading to increased osteogenesis. Alternatively, it could result from an indirect reduction of bone resorption, because osteoblasts regulate osteoclast function through paracrine signals. To distinguish between these possibilities, we performed histomorphometric analyses in 6-week-old mice from the *Prx1-Cre* and *Osx-Cre* models to obtain quantitative measures of bone formation and resorption. The data showed that bone volume per tissue volume and trabecular thickness were prominently increased on *Wtx* deficiency in both models, as were parameters of bone formation such as osteoblast number, bone formation rate per tissue volume, and mineralized surface per bone surface (Figures 2C and S3E). In contrast, in both models neither eroded surfaces nor absolute osteoclast numbers exhibited statistically significant alterations, although in the *Prx1-Cre* model there was some variability and a trend toward a decrease in eroded surfaces (Figure S4A). Additional markers of osteoclast number and activity—TRAP staining of bone sections, serum TRAP5b measurements, and qRT-PCR analysis of *TRAP* expression in bone—were unaffected by *Wtx* inactivation (Figures S4B–S4D). These results indicate that the increase in bone is primarily attributable to elevations in bone formation rather than decreased resorption. Importantly, the mineral apposition rate, which measures the osteogenic activity per osteoblast, was unchanged (Figures 2C and S3E), whereas there was evidence of an expansion of osteoblast progenitor numbers, because the trabecular bone had the characteristic immature, woven-like morphology associated with an abundance of alkaline phosphatase (ALP)-stained stromal cells (Figure 2D). Thus, the elevation in bone formation due to an increased absolute number of osteoblasts is the predominant cause of osteosclerosis in *Wtx* mutants. No changes in cell proliferation or apoptosis were detected in the *Wtx*-deficient bones analyzed at E15.5 (not shown) suggesting that Wtx acts primarily to regulate osteoblast commitment and lineage progression.

In addition to the alterations in the osteoblast lineage, the adipocyte content of long bones was sharply reduced in *Prx1-Cre;Wtx*$^{lox/Y}$ mice (Figure 2E), whereas adipocytes formed normally in *Col2a-Cre;Wtx*$^{lox/Y}$, *Osx-Cre;Wtx*$^{lox/Y}$, and *Ocn-Cre; Wtx*$^{lox/Y}$ animals (Figure S4E). Together with the loss of brown and white adipose tissue in *Wtx* null embryos (Figures 1D and S2F), this observation supports a central function for *Wtx* in adipogenesis. Collectively, these data identify *Wtx* as a critical cell autonomous regulator of osteogenic and adipogenic differentiation programs in MPCs and in early progenitors.

Wtx Inactivation Leads to Defects in Cell Fate Determination of Bone-Marrow-Derived MPCs

To functionally dissect the role of *Wtx* in lineage determination, we employed primary bone marrow-derived MPCs (BMPCs), which can be directed to undergo osteoblast or adipocyte

differentiation. BMPCs had readily detectable Wtx expression that further increased on culture under osteogenic conditions (Figure 3A). Significantly, freshly isolated BMPC cultures from *Prx1-Cre;Wtx*$^{lox/Y}$ mice exhibited a higher proportion of ALP-positive early osteoblastic cells and elevated expression of the osteoblast markers, *Runx2*, *Osx*, *Alp*, and *Ocn*, compared to wild-type cultures (Figures 3B, top, and 3C, top). These parameters increased further on in vitro culture under osteogenic conditions (Figures 3B, middle, and S3C, bottom left). Thus, Wtx normally restrains the commitment of progenitor cells toward the osteoblast lineage. However, we observed that the late differentiation of osteoblasts in vitro, as measured by the formation of alizarin red stained bone nodules, was in fact reduced in *Wtx*-deficient cells compared to wild-type controls (Figure S5A). Thus, although Wtx suppresses early osteogenic commitment, it also appears to have an additional positive role in facilitating the maturation of osteoblastic cells at later stages of differentiation.

Along with demonstrating the effects of *Wtx* ablation on osteogenesis, in vitro analyses supported the role of this gene in adipocyte differentiation. *Wtx* null BMPCs exposed to adipogenic stimulation showed severely compromised formation of oil red O-positive adipocytes (Figure 3B, bottom) and lacked induction of the adipocyte markers, *Pparg* (peroxisome proliferator activated receptor γ), and *Fabp4* (fatty acid binding protein 4) (Figure 3C, bottom right). Instead, these cells showed a striking and aberrant increase in osteoblast markers, despite culture under adipogenic conditions (Figure S5B). Pronounced increases in osteogenic commitment and defects in adipogenesis were also observed on acute inactivation of *Wtx* by *GFP-Cre* adenoviral infection of *Wtx*$^{lox/Y}$ BMPCs (Figures S5D–S5F) and by expression of shRNAs targeting *Wtx* in the ST2 MPC line (Figures 3D–3F). Importantly, *Wtx* deficiency did not cause significant alterations in overall cell number under any of the growth conditions (Figures S5C, S5F, and S5G). Taken together, these observations suggest that *Wtx* acts as a central regulator of the cell fate program in BMPCs ensuring the appropriate balance of commitment toward the osteoblast versus adipocyte lineages.

Wtx Acts Upstream of Runx2 and Pparγ in the Regulation of Osteogenic and Adipogenic Determination

Next, we sought to define the molecular basis for the altered differentiation program induced by *Wtx* inactivation. Runx2 and Pparγ are considered master regulators of osteoblastogenesis and adipogenesis, respectively, because they are required for these differentiation programs and can induce them ectopically in other cell types (Karsenty et al., 2009; Tontonoz and Spiegelman, 2008). Consistent with the increased *Runx2* mRNA expression in cultured *Wtx*-deficient mesenchymal progenitors (Figures 3C and 3F), shRNA-mediated knockdown of *Wtx* in ST2 cells resulted in upregulation of Runx2 protein levels under all growth conditions (Figure 4A). Moreover, concurrent knockdown of *Runx2* suppressed the increase in ALP staining and osteogenic gene expression induced by *Wtx* deficiency in ST2 cells (Figures 4B, upper and middle rows, S6A, and S6B), suggesting that Wtx functions upstream of Runx2 in regulating osteogenic differentiation. In contrast, *Runx2* knockdown did not restore adipogenesis in *Wtx*-deficient ST2 cells (Figures 4B, bottom row, and S6B, right).

The virtual absence of *Pparg* induction in *Wtx*-deficient mesenchymal progenitors supports a complementary function to that of Runx2 (Figures 3C and 3F). The induction of *Pparg* during adipogenesis is preceded by the upregulation of a series of early transcription factors including *Cebpb*, *Cebpd*, and *Klf5*, and is followed by expression of *Cebpa*, and the Pparγ target gene, *Fabp4* (Lefterova and Lazar, 2009). *Wtx*-deficient ST2 cells grown in adipogenic media showed normal induction of *Cebpb*, *Cebpd*, and *Klf5*, whereas, *Pparg*, *Cebpa*, and *Fabp4* were not induced, suggesting that adipogenesis is blocked at the level of *Pparg* activation (Figure 4C). Indeed, adipogenesis in *shWtx*-expressing ST2 cells was effectively restored by concurrent overexpression of *Pparg* (Figure 4D, top). *Pparg* overexpression did not override the enhanced osteogenic commitment caused by *Wtx* knockdown (Figures 4D, middle and bottom, S6C, and S6D) nor the aberrant expression of both osteogenic and adipogenic markers under adipogenic culture conditions (data not shown). Together, these data indicate that Wtx expression modulates the key osteoblast and adipocyte inducers, Runx2 and Pparγ.

Significantly, *Wtx* inactivation in vivo resulted in the same profile of molecular alterations observed in cultured BMPCs. Immunohistochemical analysis showed elevated Runx2 and Osterix expression in the perichondrium of E15.5 *Wtx*-deficient long bones, and in the trabeculae at E17.5 (Figures 4E, top, and S6E), whereas expression of the Sox9 chondrocyte lineage marker was unchanged (Figures S6E and S6F). These findings were corroborated by western blot and qRT-PCR analysis of lysates from E15.5, neonatal, and adult bones (Figures S4F, S4G, S6G, and S6H). In addition, western blot analysis revealed marked reductions in Pparγ protein levels in *Wtx*-deficient bone lysates (Figure 4F). These data suggest that Wtx functions at the early stages of BMPC differentiation to control the expression of key mediators of osteogenic and adipogenic differentiation in vivo as is observed in vitro.

Defective Cell Fate Determination of *Wtx*-Deficient BMPCs Is Due to Aberrant β-Catenin Activation

Activation of the canonical Wnt signaling pathway governs the cell fate program of MPCs, enhancing osteogenesis and inhibiting adipogenesis in part through the regulation of expression and transcriptional activity of both Runx2 and Pparγ (Takada et al., 2009). Wtx itself has been implicated in the regulation of β-catenin through its interaction with the APC degradation complex (Major et al., 2007). We therefore tested for alterations in Wnt pathway components in *Wtx* mutant BMPCs and mice. *Prx1-Cre;Wtx*$^{lox/Y}$ BMPCs showed increased total and active β-catenin (ABC) compared to control cells under noninducing, osteogenic, and adipogenic conditions (Figure 5A). Correspondingly the expression of multiple transcriptional targets of β-catenin, including *Axin2* and *Tcf1*, was elevated in these cells (Figure 5B and not shown). shRNAs targeting *Wtx* also caused acute induction of β-catenin and its target genes in ST2 cells (Figures 5C and 5D). Addition of the proteasome inhibitor, MG132 equalized β-catenin levels, consistent with regulation of β-catenin stability by Wtx (Figure S7A). β-catenin mRNA levels showed no increase in *Wtx*-deficient ST2 cells (not shown). As expected, the increase in β-catenin associated with *Wtx* knockdown was not affected by suppression of *Runx2* or overexpression *Pparg* (Figure S7B).

We next sought to directly test the contribution of aberrant β-catenin activity to the defects caused by *Wtx* inactivation in BMPCs. shRNA-mediated knockdown of β-catenin suppressed the abnormal osteogenic commitment of *Wtx*-deficient ST2 cells under all growth conditions (Figure 5E, upper three rows). Moreover, it restored their capacity for adipogenic differentiation (Figure 5E, bottom row), and normalized the expression of Runx2 polypeptide and *Pparg* mRNA (Figures S7B and S7D); additional osteoblast-selective and adipocyte-selective genes and β-catenin target genes showed similar responses (Figures S7C and S7D). Collectively, these data support a model in which *Wtx* inactivation in BMPCs leads to stabilization of β-catenin and consequent disruption of both osteogenesis and adipogenesis, in part through modulation of Runx2 and Pparγ activity.

Importantly, there was evidence for pronounced activation of canonical Wnt signaling on *Wtx* inactivation in vivo. *Wtx*-deficient embryos displayed an increased number of $Tcf1^+$ and $Lef1^+$ cells within the perichondrium at E14.5 and in the developing trabeculae at E17.5 (Figures 6A and S7E), indicating that the Wnt pathway was aberrantly activated in mesenchymal progenitors and osteoblast precursors. In further support of these findings, western blot analysis showed increased *β-catenin* protein levels in E15.5 and neonatal *Wtx*-deficient bone lysates (Figure 6B).

To determine the relevance of *β-catenin* dysregulation to the skeletal defects caused by *Wtx* inactivation in vivo, we crossed *Prx1-Cre;*$Wtx^{lox/Y}$ mice with a conditional *β-catenin* (*β-catenin*^{lox}) knockout strain. *Prx1-Cre;β-catenin*$^{lox/+}$; $Wtx^{+/Y}$ control mice showed slight reductions in bone size, but otherwise exhibited normal skeletal development. Importantly, *Prx1-Cre;β-catenin*$^{lox/+}$*;*$Wtx^{lox/Y}$ mice had comparable skeletal morphology and cortical bone formation; the defects caused by *Wtx* inactivation—misalignment of the ribs along the sternum, malformation of the deltoid tuberosity and increase in cortical bone—were mitigated by concurrent reductions in *β-catenin* gene dosage indicating that heterozygous inactivation of *β-catenin* largely rescues the bone phenotypes associated with *Wtx* deficiency (Figures 6C, S7F, and S7G). Hence, Wtx-mediated suppression of canonical Wnt signaling is central to the control of cell fate in MPCs in the bone marrow.

Wtx Inactivation Causes Delayed Maturation of Committed Osteoblasts Independently of β-Catenin

Despite the demonstrated modulation of β-catenin by Wtx in BMPC differentiation, the two genes have distinct roles in later stages of osteogenesis. Constitutive activation of canonical Wnt signaling by activated β-catenin enhances both early as well as later osteogenic processes (Krause et al., 2010; Yan et al., 2009). In contrast, as noted above (Figure S5A), the enhanced osteoblastic commitment resulting from *Wtx* suppression in vitro is ultimately followed by delayed mineralization. To address whether inactivation of *Wtx* results in delays in terminal differentiation in vivo, we examined skeletal preparations of *Wtx*-null and wild-type mice at different embryonic time points. This analysis revealed that *Wtx* inactivation caused a deficiency in intramembranous and endochondral bone ossification (Figures 7A and 7B). In the calvarium, this was characterized by abnormally distant ossification fronts in the perinatal cranial vault and by malformation of the postnatal suture (Figures 7A and S8A). *Wtx*-deficient long bones exhibited delayed mineralization at E14.5 (Figure 7B),

unmineralized regions below the growth cartilage and discontinuous cortical bone layer at E15.5 (Figure S8B, left), and decreased mineralization of the trabecular area perinatally (Figures 7B and S8B, right). Similar mineralization defects were observed in *Osx-Cre;* $Wtx^{lox/Y}$ but not in *Ocn-Cre;*$Wtx^{lox/Y}$ animals (Figure S8C and data not shown). There was also evidence for delayed mineralization in the homeostasis of adult long bones in *Prx1-Cre;*$Wtx^{lox/Y}$ mice as reflected by a 2-fold increase in osteoid volume per bone volume (OV/TV) (Figure S8D). Thus, despite the increase in osteoblasto-genesis and ensuing sclerotic phenotype, there is a persistence of unmineralized elements in *Wtx*-deficient bone.

Based on these findings, we examined the impact of *Wtx* inactivation on the later stages of osteoblast differentiation. Expression of *Wtx*-targeted shRNA into the committed osteoblastic MC3T3-E1 cell line resulted in delayed osteoblast differentiation as reflected by reductions in ALP and alizarin red staining, and in osteoblast gene expression (Figures 7C and 7D and data not shown). Together, these results further support a positive role for Wtx in the terminal differentiation of committed osteoblast precursors, an effect that is clearly distinct from the earlier function of Wtx in suppressing the commitment of MPCs to the osteoblast lineage.

The preceding results appear inconsistent with Wtx functioning as a negative regulator of canonical Wnt signaling in committed osteoblasts. Therefore, we evaluated the β-catenin levels in BMPCs at multiple time points and in MC3T3-E1 cells. Notably, whereas β-catenin levels were upregulated in *Prx1-Cre;*$Wtx^{lox/Y}$ BMPCs before induction or up to 6 days after growth in osteogenic media, levels were significantly reduced at later time points of osteogenic induction in the *Wtx*-deficient BMPC cultures compared to controls (Figure 8A); similar reductions in β-catenin were observed on acute inactivation of *Wtx* in MC3T3-E1 cells (Figure 8A). *Axin2* and *Tcf1* mRNA levels showed a comparable profile (Figure 8B). Consistent with these in vitro studies showing β-catenin activation in *Wtx* null early precursors but not in committed precursors, *Wtx* null embryos displayed an increased number of $Tcf1^{+}$ cells in the developing trabeculae where precursors actively differentiate, but not in the bone shaft where mature osteoblasts reside (Figure S7E). Significantly, neither reduction in β-catenin expression using shRNA (Figure 8C) nor stabilization of β-catenin via treatment with the GSK3 inhibitor, bromo-indirubin 3′ oxime (BIO) (Figure 8D), rescued osteoblast differentiation caused by *Wtx* knockdown in MC3T3-E1 cells. Thus, unlike the specification defects caused by *Wtx* deficiency in early BMPCs, the impairment in maturation of committed osteoblastic cells appears independent of β-catenin deregulation.

Collectively, the data indicate that the overgrowth of *Wtx* null bones reflects two processes; increased commitment of MPCs to the osteoblast lineage coupled with a subsequent delay in the terminal differentiation of committed osteoblastic cells. The alterations in lineage commitment in MPCs are driven by increased β-catenin signaling, whereas the effects on differentiation or lineage maintenance involve other pathways. Wnt regulation by Wtx is thus stage-dependent and its changing properties are associated with distinct aspects of MPC commitment and differentiation (Figure 8E).

DISCUSSION

Pediatric cancers provide a fascinating window into the link between normal tissue differentiation and tumorigenesis. In contrast to adult cancers, pediatric cancers like Wilms tumor display relatively stable genomic landscapes and often arise from tissue-specific progenitors that aberrantly recapitulate features of development, including multi-lineage differentiation. The mouse knockout of the first Wilms tumor suppressor gene, *Wt1*, provided important insights into the embryonic differentiation of the kidney, as well as heart, mesothelium, spleen, and hematopoietic tissues (Kreidberg et al., 1993; Rivera and Haber, 2005; Martinez-Estrada et al., 2010). We now report that inactivation of the second Wilms tumor suppressor, *Wtx*, in the mouse results in profound abnormalities in bone, adipose tissue, kidneys, heart and spleen. Our data shows that alterations in bone and adipose tissue are due to direct functions of Wtx in the commitment and lineage progression of MPCs and, together with the constellation of defects in *Wtx* null mice, suggest that *Wtx* may act more broadly as a critical regulator of differentiation in multiple embryonic mesenchymal lineages.

Skeletal abnormalities—the phenotypes we studied in most detail—parallel those associated with germline inactivation of *WTX* in the human X-linked disorder OSCS (Jenkins et al., 2009) and appear to be linked to sequential roles of *Wtx* in the commitment of MPCs and in the differentiation of osteoblast precursors. The OSCS phenotype in long bones can be recapitulated by targeted *Wtx* inactivation in the earliest mesenchymal progenitors (e.g., in *Prx1-Cre*;$Wtx^{lox/Y}$ mice) where the absence of *Wtx* contributes to bone overgrowth by increasing commitment toward osteoblastogenesis. In contrast, specific inactivation of *Wtx* in mature osteoblasts (e.g., in *Ocn-Cre*;$Wtx^{lox/Y}$ mice) does not cause any skeletal defects. Significantly, macrocephaly in *Wtx null* mice is associated with distant ossification fronts and a large fontanelle, and osteosclerosis of the long bones is preceded by defects in early embryonic bone formation, suggesting an overall delay in bone development. Our in vitro studies appear to recapitulate the bone phenotypes because *Wtx* inactivation results in increased commitment of BMPCs to the osteoblast lineage coupled with impairment or delay in the terminal differentiation of committed osteoblasts. We thus propose a model whereby children with OSCS suffer from the combination of early and late effects, including bone overgrowth through the progressive expansion of the osteoblastic lineage coupled with the accumulation of immature elements (Figure 8E). In vivo, the expanded osteoblast precursor pool presumably compensates for the delayed or impaired osteoblast maturation over time, leading to age-dependent increases in bone formation. The endochondral bone phenotypes observed in *Wtx*-deficient mice are also likely to be influenced by complex interactions between MPCs, chondrocytes, and osteoblastic cells, as well as potential alterations in the osteoclasts.

Wtx has been implicated in Wnt signaling, as a component of the β-catenin destruction complex, and our experiments show that its role in the lineage allocation of BMPCs is linked to regulation of this pathway. However, the effects of β-catenin and Wtx on later stages of bone formation are clearly distinct. Activation of the canonical Wnt signaling pathway induces entry of MPCs into the osteochondroprogenitor lineage at the expense of the adipogenic lineage (Akune et al., 2004; Ross et al., 2000), and sustained β-catenin

activity in the osteochondroprogenitors further directs allocation into the osteoblast lineage while preventing chondrocyte specification (Day et al., 2005; Hill et al., 2005). Correspondingly, it has been proposed that β-catenin levels must diminish for chondrogenesis to occur (Case and Rubin, 2010). *Wtx* null mice show aberrant osteogenic commitment coupled with impaired adipocyte formation, whereas chondrocytes form abundantly, consistent with Wtx acting as a stage-specific repressor of β-catenin activity with an important role of this regulatory pathway that is restricted to the early mesenchymal progenitors and osteoblast precursors. In addition to its function in lineage specification, β-catenin activity in committed osteoblasts enhances bone accumulation through effects on osteoclast differentiation and on mature osteoblast activity (Glass et al., 2005; Yan et al., 2009). In contrast, *Wtx*-deficient adult mice show increased bone formation and osteoblastogenesis without significant alterations in bone resorption, suggesting that Wtx is not a critical negative regulator of β-catenin in this context. Moreover, *Wtx* deficiency causes delays in the closure of the cranial suture whereas β-catenin activation driven by *Axin2* deficiency has the opposite phenotype (Yu et al., 2005), indicating that Wtx has functions that are independent of β-catenin regulation in osteoblast differentiation. Our in vitro studies recapitulate this developmental stage specific regulation of β-catenin by Wtx. In summary, Wtx appears to be a negative regulator of β-catenin in undifferentiated MPCs and osteoblast precursors, but not in differentiated osteoblasts, thereby accounting for the distinct effects of β-catenin and Wtx on multiple stages of bone formation.

Wnt pathway activation is both a trigger and consequence of bone formation: whereas the increased β-catenin levels in early precursors may be directly attributable to loss of Wtx-mediated degradation, the reduced β-catenin levels observed in later stages of bone development are presumably the indirect result of Wtx-mediated delay in bone maturation. We thus propose a model for stage-specific effects of Wtx on bone and fat differentiation, including a developmentally restricted effect on Wnt/β-catenin signaling (Figure 8E).

In addition to osteosclerosis, other phenotypes associated with germline *WTX* inactivation in humans with OSCS are highly variable, likely due to genetic modifiers and the fact that most documented cases involve female carriers (who are mosaic due to random X chromosome inactivation) and rare males with attenuated presentations (Jenkins et al., 2009). Our analysis of *Wtx* null mice identifies a well-defined set of malformations that involve kidneys, adipose tissue, heart, and spleen, in addition to the skeleton. Although our studies did not address the functions of *Wtx* in these other tissues in detail, we note that these developmental defects appear to be restricted to organs originating from mesenchymal progenitors. Moreover, Wilms tumor, the other major abnormality associated with *WTX* inactivation in humans, is thought to arise from kidney MPCs.

Wilms tumor has not been reported in children with OSCS, nor did we observe the development of kidney tumors in $Wtx^{+/}$ mice (eight mice analyzed between 40 to 80 weeks of age). Our data in the mouse suggest that the absence of tumors may reflect complex roles of Wtx in kidney development that lead most commonly to either agenesis or overgrowth, but also to some cases of hypoplasia. Of note, we have observed some strain dependence in the phenotypes observed, with increased agenesis in a C57BL/6 background compared to a 129SV background (data not shown); the variable penetrance of renal agenesis phenotypes

has been extensively documented (Brodbeck and Englert, 2004). Our analysis shows that Wtx is required to prevent apoptosis of the early renal mesenchyme, whereas the kidneys that do form in *Wtx* null mice provide a window into the effect of Wtx at later stages of renal differentiation. The increased size of these kidneys is associated with accumulation of subcapsular Six2-positive, multipotent mesenchymal precursors, a cell population that is also commonly expanded in Wilms tumors (Li et al., 2002). This observation raises the possibility that *WTX* inactivation may contribute to tumorigenesis in part by increasing the pool of mesenchymal target cells at risk for transformation. Such an expansion of renal precursors has been reported in the kidneys of children with Beckwith-Wiedemann syndrome, a fetal overgrowth phenotype linked to IGF2 expression and associated with Wilms tumor in ~5% of cases (Ohlsson et al., 1993; Weksberg et al., 1993). Interestingly, bilateral multifocal expansions of renal precursors have recently been noted in a patient with OSCS (Fukuzawa et al., 2010).

The multifaceted properties of Wtx in distinct cell types are shared by other tumor suppressors. Recently, the retinoblastoma susceptibility gene *RB*, involved in cell cycle progression and rate limiting for tumorigenesis in neural crest-derived retinoblasts, has similarly been implicated in cell fate specification of MPCs (Calo et al., 2010). The effect of *Rb* inactivation in MPCs appears to be reciprocal to that of *Wtx* loss, favoring adipocyte differentiation at the expense of osteoblast commitment. These lineage dependent effects of *Rb* are insufficient to drive tumorigenesis, but may impact the spectrum of mesenchymal tumors in the setting of concomitant *Tp53* inactivation.

In summary, we have identified functional properties of the *Wtx* tumor suppressor, pointing to critical developmental roles in multiple organs derived from MPCs. In the bone marrow MPCs, Wtx differentially regulates lineage specification, as well as the subsequent progression of differentiation programs, thereby maintaining the balance between mature mesenchyme-derived osteoblasts and adipocytes. Loss of *Wtx* in MPCs thus leads to a pronounced osteogenic phenotype. In other tissues such as kidney, Wtx inactivation leads either to apoptosis of mesenchymal cells and failure of organogenesis, or alternatively to organomegaly, associated with increased precursor populations. Together, these observations point to a complex network of mesenchymal differentiation pathways controlled by WTX, whose deregulation contributes to human developmental abnormalities and pediatric cancer.

EXPERIMENTAL PROCEDURES

Immunohistochemistry

Immunohistochemistry was performed using standard protocols with the following antibodies: Six2 (Proteintech, 1:200), cleaved caspase 3 (Cell Signaling Technologies, 1:200), Runx2 (Sigma, 1:500), and Sox9 (Sigma, 1:200). Briefly, sections were deparaffinized using Xylene for 30 min and antigen retrieval was performed by boiling in 10 mM sodium citrate with 0.05% Tween-20 for 15 min or by pressure cooking. Primary antibodies were incubated overnight at 4°C or 1 hr at room temperature and secondaries for 2 hr at room temperature. Signals were detected using the ABC kit for immunoperoxidase staining (Vector Laboratories).

Cell Culture

BMPCs were extracted from neonatal femurs, tibiae, and humerus and plated in 10-cm dishes containing α-MEM supplemented with 20% fetal bovine serum (FBS). Cells were expanded in 15-cm dishes for 2 weeks. Eighty percent confluent dishes were harvested and cells were plated for differentiation assays. ST2 and MC3T3-E1 cells were maintained in α-MEM supplemented with 10% FBS.

Differentiation Assays

For osteogenic differentiation, BMPCs, ST2 and MC3T3-E1 cells were plated at a density of 5500 cells/cm^2. BMPCs and MC3T3-E1 cells were grown in osteogenic medium (α-MEM/20% FBS containing 10 μM β-glycerol-phosphate, 50 μg/ml ascorbic acid, and 10 nM dexamethasone). ST2 were grown in osteogenic medium supplemented with 300 ng/ml of recombinant BMP2. For adipogenic differentiation of BMPCs and ST2 cells were plated at a density of 15,000 cells/cm^2, grown to confluence, stimulated in adipogenic induction medium (DMEM/10% FBS containing 50 μM dexamethasone, 100 μM indo-methacin, 500 μM IBMX, 10 μg/ml insulin) followed by adipogenic maintenance medium (DMEM/10% FBS containing 50 μM dexamethasone, 10 μg/ml insulin, 5 μM rosiglitazone). BIO or methyl-bromo-indirubin 3′oxime (MeBIO) was added to MC3T3-E1 cells at a 0.8 μM final concentration every 2 days.

Cell Staining

Cells were fixed with 4% paraformaldehyde and stained for ALP (BCIP/NBT liquid substrate; Sigma B1911), bone nodule formation (1 mg/ml alizarin red solution pH5.5), lipid accumulation (2 μg/ml oil red O solution), and total cell number (0.5 μg/ml 4′,6-diamidino-2-phenylindole-DAPI solution).

Supplementary Material

Refer to Web version on PubMed Central for supplementary material.

Acknowledgments

This work was supported by grants from Alex's Lemonade Stand Foundation and the Sidney Kimmel Foundation to N.B., and from the NCI (R37CA058596 and P50CA101942) and the Howard Hughes Medical Institute to D.H. A.M. is the recipient of a Postdoctoral Fellowship from Fonds de la Recherche en Santé du Québec (FRSQ) and from the Kidney Research Scientist Core Education and National Training Program (KRESCENT). M.N.R. is supported by awards from the NIDDK (K08DK080175), the Burroughs Welcome Fund, the Howard Hughes Medical Institute, and Massachusetts General Hospital. We thank K. Hochedlinger, Tim Ahfeldt, and Chad Cowan for helpful discussions and provision of reagents, K. Cheng for assistance with the Wtx targeting vector, Cell Signaling Technology for developing anti-WTX antibodies, J. Park and A. Stone for technical assistance, J. Wu for assistance with bone density measurements, K. Atkin for bone histology, A. Guimaraes and B. Marinelli for PET-CT imaging, A. Wolfer for critical reading of the manuscript, J. Fitamant for graphic design, and members of the Bardeesy and Haber labs for suggestions and advice.

REFERENCES

Akune T, Ohba S, Kamekura S, Yamaguchi M, Chung UI, Kubota N, Terauchi Y, Harada Y, Azuma Y, Nakamura K, et al. PPARgamma insufficiency enhances osteogenesis through osteoblast formation from bone marrow progenitors. J. Clin. Invest. 2004; 113:846–855. [PubMed: 15067317]

Boyle WJ, Simonet WS, Lacey DL. Osteoclast differentiation and activation. Nature. 2003; 423:337–342. [PubMed: 12748652]

Brodbeck S, Englert C. Genetic determination of nephrogenesis: the Pax/Eya/Six gene network. Pediatr. Nephrol. 2004; 19:249–255. [PubMed: 14673635]

Calo E, Quintero-Estades JA, Danielian PS, Nedelcu S, Berman SD, Lees JA. Rb regulates fate choice and lineage commitment in vivo. Nature. 2010; 466:1110–1114. [PubMed: 20686481]

Case N, Rubin J. Beta-catenin—a supporting role in the skeleton. J. Cell. Biochem. 2010; 110:545–553. [PubMed: 20512915]

Day TF, Guo X, Garrett-Beal L, Yang Y. Wnt/beta-catenin signaling in mesenchymal progenitors controls osteoblast and chondrocyte differentiation during vertebrate skeletogenesis. Dev. Cell. 2005; 8:739–750. [PubMed: 15866164]

Fukuzawa R, Holman SK, Chow CW, Savarirayan R, Reeve AE, Robertson SP. WTX mutations can occur both early and late in the pathogenesis of Wilms tumour. J. Med. Genet. 2010; 47:791–794. [PubMed: 20679664]

Glass DA 2nd, Bialek P, Ahn JD, Starbuck M, Patel MS, Clevers H, Taketo MM, Long F, McMahon AP, Lang RA, Karsenty G. Canonical Wnt signaling in differentiated osteoblasts controls osteoclast differentiation. Dev. Cell. 2005; 8:751–764. [PubMed: 15866165]

Grohmann A, Tanneberger K, Alzner A, Schneikert J, Behrens J. AMER1 regulates the distribution of the tumor suppressor APC between microtubules and the plasma membrane. J. Cell Sci. 2007; 120:3738–3747. [PubMed: 17925383]

Hill TP, Spater D, Taketo MM, Birchmeier W, Hartmann C. Canonical Wnt/beta-catenin signaling prevents osteoblasts from differentiating into chondrocytes. Dev. Cell. 2005; 8:727–738. [PubMed: 15866163]

Jenkins ZA, van Kogelenberg M, Morgan T, Jeffs A, Fukuzawa R, Pearl E, Thaller C, Hing AV, Porteous ME, Garcia-Minaur S, et al. Germline mutations in WTX cause a sclerosing skeletal dysplasia but do not predispose to tumorigenesis. Nat. Genet. 2009; 41:95–100. [PubMed: 19079258]

Karsenty G, Kronenberg HM, Settembre C. Genetic control of bone formation. Annu. Rev. Cell Dev. Biol. 2009; 25:629–648. [PubMed: 19575648]

Kobayashi A, Valerius MT, Mugford JW, Carroll TJ, Self M, Oliver G, McMahon AP. Six2 defines and regulates a multipotent self-renewing nephron progenitor population throughout mammalian kidney development. Cell Stem Cell. 2008; 3:169–181. [PubMed: 18682239]

Koesters R, Ridder R, Kopp-Schneider A, Betts D, Adams V, Niggli F, Briner J, von Knebel Doeberitz M. Mutational activation of the beta-catenin proto-oncogene is a common event in the development of Wilms' tumors. Cancer Res. 1999; 59:3880–3882. [PubMed: 10463574]

Krause U, Harris S, Green A, Ylostalo J, Zeitouni S, Lee N, Gregory CA. Pharmaceutical modulation of canonical Wnt signaling in multipo-tent stromal cells for improved osteoinductive therapy. Proc. Natl. Acad. Sci. USA. 2010; 107:4147–4152. [PubMed: 20150512]

Kreidberg JA, Sariola H, Loring JM, Maeda M, Pelletier J, Housman D, Jaenisch R. WT-1 is required for early kidney development. Cell. 1993; 74:679–691. [PubMed: 8395349]

Lefterova MI, Lazar MA. New developments in adipogenesis. Trends Endocrinol. Metab. 2009; 20:107–114. [PubMed: 19269847]

Li CM, Guo M, Borczuk A, Powell CA, Wei M, Thaker HM, Friedman R, Klein U, Tycko B. Gene expression in Wilms' tumor mimics the earliest committed stage in the metanephric mesenchymal-epithelial transition. Am. J. Pathol. 2002; 160:2181–2190. [PubMed: 12057921]

Logan M, Martin JF, Nagy A, Lobe C, Olson EN, Tabin CJ. Expression of Cre Recombinase in the developing mouse limb bud driven by a Prxl enhancer. Genesis. 2002; 33:77–80. [PubMed: 12112875]

Major MB, Camp ND, Berndt JD, Yi X, Goldenberg SJ, Hubbert C, Biechele TL, Gingras AC, Zheng N, Maccoss MJ, et al. Wilms tumor suppressor WTX negatively regulates WNT/beta-catenin signaling. Science. 2007; 316:1043–1046. [PubMed: 17510365]

Martinez-Estrada OM, Lettice LA, Essafi A, Guadix JA, Slight J, Velecela V, Hall E, Reichmann J, Devenney PS, Hohenstein P, et al. Wt1 is required for cardiovascular progenitor cell formation

through transcriptional control of Snail and E-cadherin. Nat. Genet. 2010; 42:89–93. [PubMed: 20023660]

Ohlsson R, Nystrom A, Pfeifer-Ohlsson S, Tohonen V, Hedborg F, Schofield P, Flam F, Ekstrom TJ. IGF2 is parentally imprinted during human embryogenesis and in the Beckwith-Wiedemann syndrome. Nat. Genet. 1993; 4:94–97. [PubMed: 8513333]

Perdu B, de Freitas F, Frints SG, Schouten M, Schrander-Stumpel C, Barbosa M, Pinto-Basto J, Reis-Lima M, de Vernejoul MC, Becker K, et al. Osteopathia striata with cranial sclerosis due to WTX gene defect. J. Bone Miner. Res. 2010; 25:82–90. [PubMed: 20209645]

Pritchard-Jones K, Fleming S, Davidson D, Bickmore W, Porteous D, Gosden C, Bard J, Buckler A, Pelletier J, Housman D, et al. The candidate Wilms' tumour gene is involved in genitourinary development. Nature. 1990; 346:194–197. [PubMed: 2164159]

Rivera MN, Haber DA. Wilms' tumour: connecting tumorigenesis and organ development in the kidney. Nat. Rev. Cancer. 2005; 5:699–712. [PubMed: 16110318]

Rivera MN, Kim WJ, Wells J, Driscoll DR, Brannigan BW, Han M, Kim JC, Feinberg AP, Gerald WL, Vargas SO, et al. An X chromosome gene, WTX, is commonly inactivated in Wilms tumor. Science. 2007; 315:642–645. [PubMed: 17204608]

Rivera MN, Kim WJ, Wells J, Stone A, Burger A, Coffman EJ, Zhang J, Haber DA. The tumor suppressor WTX shuttles to the nucleus and modulates WT1 activity. Proc. Natl. Acad. Sci. USA. 2009; 106:8338–8343. [PubMed: 19416806]

Rosen CJ, Ackert-Bicknell C, Rodriguez JP, Pino AM. Marrow fat and the bone microenvironment: developmental, functional, and pathological implications. Crit. Rev. Eukaryot. Gene Expr. 2009; 19:109–124. [PubMed: 19392647]

Ross SE, Hemati N, Longo KA, Bennett CN, Lucas PC, Erickson RL, MacDougald OA. Inhibition of adipogenesis by Wnt signaling. Science. 2000; 289:950–953. [PubMed: 10937998]

Takada I, Kouzmenko AP, Kato S. Wnt and PPARgamma signaling in osteoblastogenesis and adipogenesis. Nat. Rev. Rheumatol. 2009; 5:442–447. [PubMed: 19581903]

Tontonoz P, Spiegelman BM. Fat and beyond: the diverse biology of PPARgamma. Annu. Rev. Biochem. 2008; 77:289–312. [PubMed: 18518822]

Weksberg R, Shen DR, Fei YL, Song QL, Squire J. Disruption of insulin-like growth factor 2 imprinting in Beckwith-Wiedemann syndrome. Nat. Genet. 1993; 5:143–150. [PubMed: 8252039]

Yan Y, Tang D, Chen M, Huang J, Xie R, Jonason JH, Tan X, Hou W, Reynolds D, Hsu W, et al. Axin2 controls bone remodeling through the beta-catenin-BMP signaling pathway in adult mice. J. Cell Sci. 2009; 122:3566–3578. [PubMed: 19737815]

Yu HM, Jerchow B, Sheu TJ, Liu B, Costantini F, Puzas JE, Birchmeier W, Hsu W. The role of Axin2 in calvarial morphogenesis and craniosynostosis. Development. 2005; 132:1995–2005. [PubMed: 15790973]

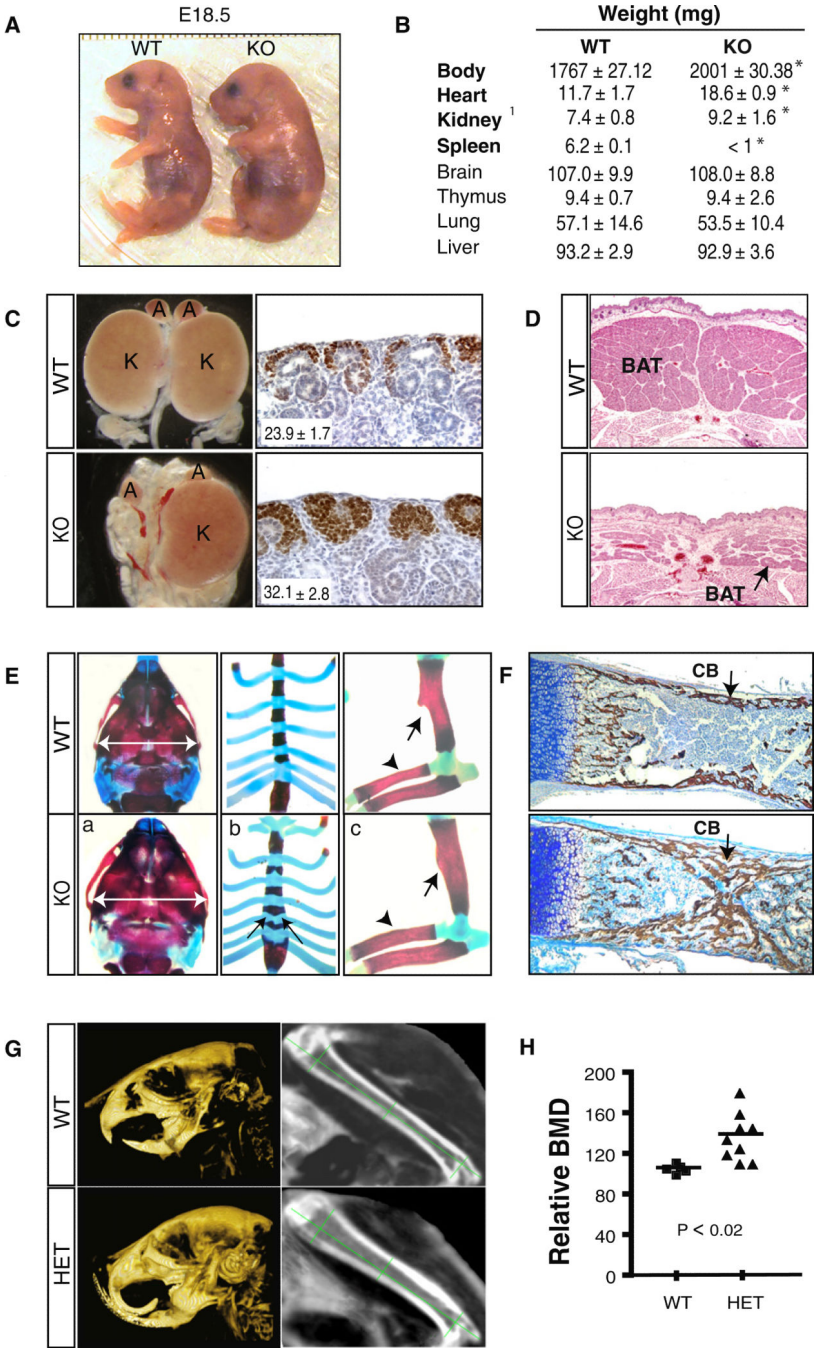

Figure 1. Germline Inactivation of *Wtx* Leads to Defects in Multiple Mesenchyme-Derived Tissues

(A) Gross images of E18.5 wild-type (WT) and *Wtx* null (KO) embryos.

(B) Weight of neonatal organs; organs showing significant differences are indicated in bold, *$p < 0.01$. [1]*Wtx* null kidneys were either absent or heavier than wild-type counterparts.

(C) Left: Representative gross images of neonatal kidneys (K) and adrenals (A) showing unilateral agenesis in a *Wtx* null mouse. Right: Immunohistochemistry (IHC) showing increased numbers of $Six2^+$ cells in neonatal *Wtx* null kidneys; quantification of the $Six2^+$ aggregates is shown at the bottom ($p < 0.001$).

(D) Hematoxylin and eosin (H&E) staining of the interscapular region at E18.5 showing paucity of brown adipose tissue (BAT, arrow) in *Wtx* KO mice.
(E) Alizarin red/Alcian blue stained neonatal skeletal preparations. *Wtx* KO mice show: (a) enlargement of the skull, (b) dysplasia of the sternum, and (c) enlarged and bowed radius and ulna (arrowhead) and absence of the deltoid tuberosity (arrow).
(F) Von Kossa staining of mineralized bone matrix in neonatal femurs; cortical bone (CB).
(G) PET-CT images of skull (left) and femur (right) of 4-month-old wild-type and *Wtx* heterozygous (HET) mice.
(H) Bone mineral density (BMD) of adult skulls. See also Figures S1 and S2.

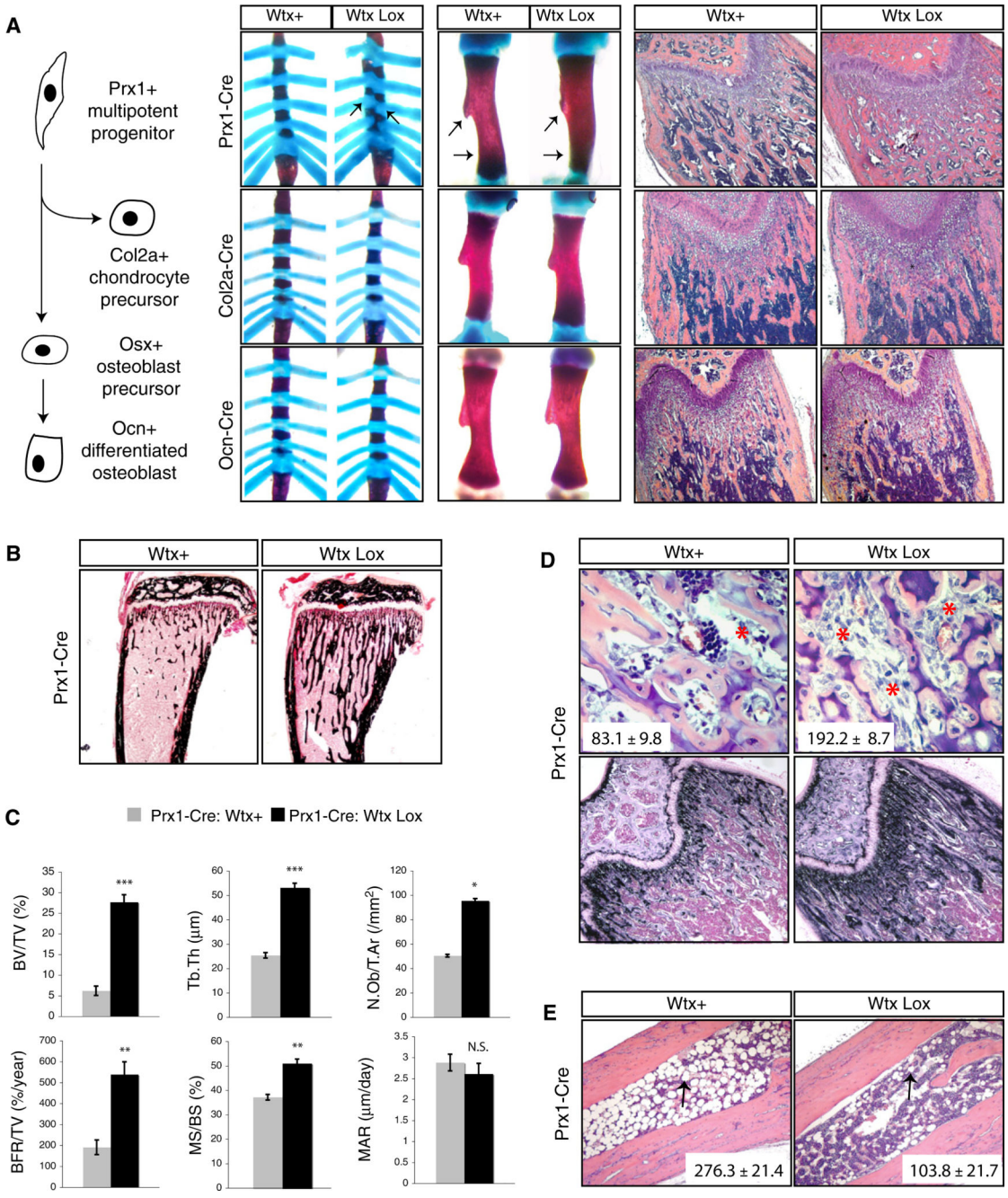

Figure 2. Targeted Inactivation of *Wtx* in Mesenchymal Progenitors Causes Osteosclerosis and Impaired Adipogenesis

(A) *Wtx*^{lox} mice were crossed with the *Prx1-Cre*, *Col2a-Cre*, or *Ocn-Cre* strains to inactivate Wtx at different stages of skeletal development (schematic diagram). Alizarin red/Alcian blue stained neonatal sternums (left) and femurs (center), and H&E stained adult femurs (right) from the indicated models. *Prx1-Cre;Wtx*$^{lox/Y}$ mice show dysplasia of sternum and femur (arrows) and marked osteosclerosis.

(B–E) Analysis of the *Prx1-Cre* model at age 6 weeks. Von Kossa staining of tibiae is shown in (B). Histomorphometry showing bone volume/tissue volume (BV/TV), trabecular

thickness (Tb.Th), osteoblast number/tissue surface (N.Ob/T.Ar), bone formation rate per tissue volume (BFR/TV), mineralized surface per bone surface (MS/BS), and mineral apposition rate (MAR) is shown in (C). ***$p < 0.001$, **$p < 0.01$, *$p < 0.05$, N.S., not significant. In (D), upper panel is of H&E showing stromal cells (*) in trabecular bone; the numbers of stromal cells per field are indicated. Lower (D) is an alkaline phosphatase staining (ALP) of trabecular bone. H&E staining of distal tibiae is shown in (E) (arrows: adipocytes). See also Figures S3 and S4.

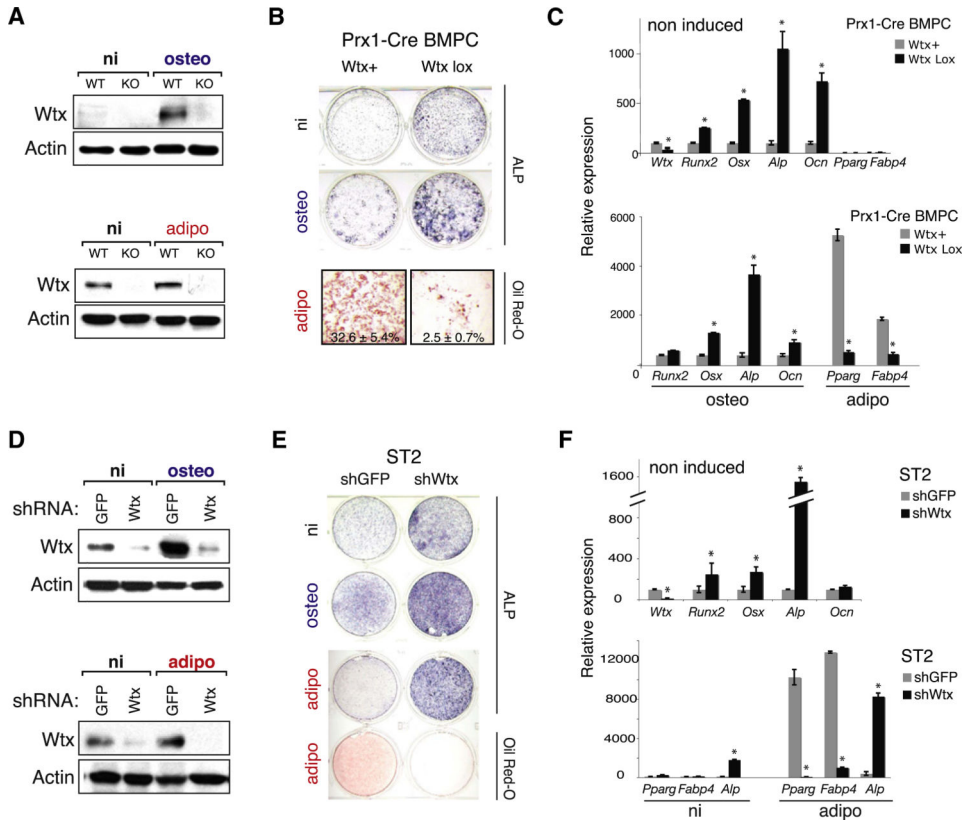

Figure 3. *Wtx* Regulates Osteoblastogenesis and Adipogenesis in BMPCs

(A–C) Wild-type and *Wtx* KO BMPCs were grown in noninducing (ni) and osteogenic (osteo) conditions for 6 days or in adipogenic (adipo) conditions for 12 days, respectively and analyzed by western blot for Wtx expression (A), ALP (B, top and middle) and oil red O staining (B, bottom; % stained cells are indicated), and qRT-PCR analysis for expression of osteoblast-selective genes and adipocyte-selective genes (C).

(D–F) ST2 cells expressing *shGFP* (control) or *shWtx* were grown under noninducing (ni) and osteogenic (osteo) conditions for 6 days, or in adipogenic (adipo) conditions for 12 days; cells were analyzed for Wtx expression by western blot (D), ALP and oil red O staining as indicated (E), and expression of osteoblast-selective (F, top) and adipocyte-selective genes (F, bottom). *$p < 0.05$. See also Figure S5.

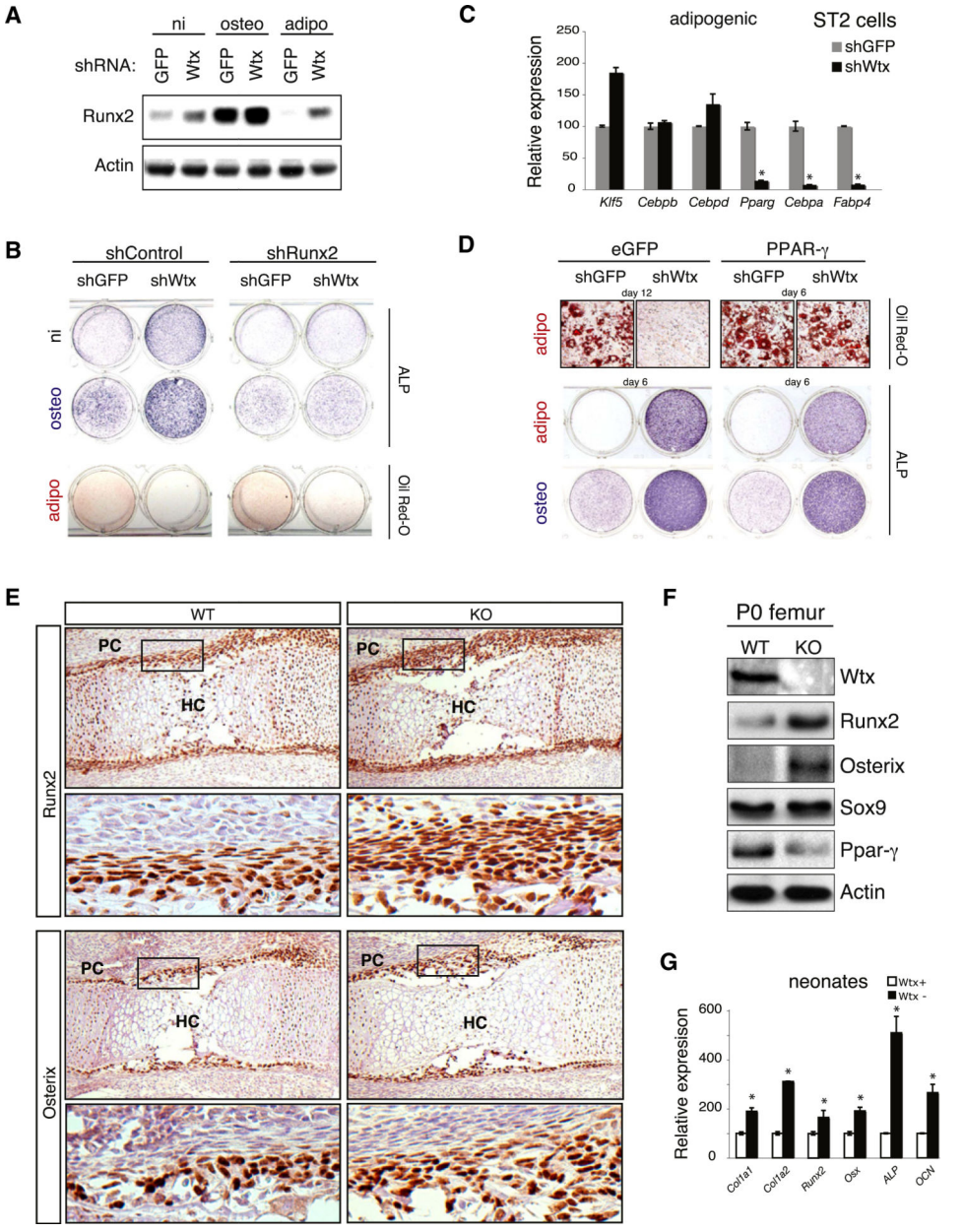

Figure 4. Wtx Acts Upstream of Runx2 and Pparγ to Control Osteogenic and Adipogenic Fate Determination

(A) Runx2 expression detected by western blot in ST2 cells expressing *shGFP* or *shWtx*.

(B) ST2 cells expressing combinations of shRNAs targeting control (*GFP*), *Wtx*, and *Runx2* were grown under noninducing (ni) and osteogenic (osteo) conditions for 6 days, or in adipogenic (adipo) conditions for 12 days, and examined for ALP staining (top and center rows) and oil red O (bottom row).

(C) ST2 cells expressing *shGFP* or *shWtx* were grown under adipogenic conditions and analyzed for adipogenic differentiation markers. *$p < 0.05$.

(D) ST2 cells overexpressing either control *GFP* or *PPARγ*, in combination with either *shGFP* or *shWtx*, were grown under indicated conditions and analyzed for oil red O staining

(top), and ALP staining (middle and bottom). Oil red O staining was performed on adipogenic day 12 in the *eGFP*-expressing cells and on day 6 in PPARγ-expressing cells.
(E) IHC in E15.5 humerus showing increases in Runx2 and Osx staining in *Wtx* KO mice compared to WT controls. HC, hypertrophic chondrocytes; PC, perichondrium.
(F) Osteogenic (Runx2 and Osterix), chondrogenic (Sox9), and adipogenic (Pparγ) lineage marker expression detected by western blot of neonatal WT and *Wtx* KO femur.
(G) WT and *Wtx* KO neonatal long bones were analyzed for osteoblast-selective gene expression by qRT-PCR. See also Figure S6.

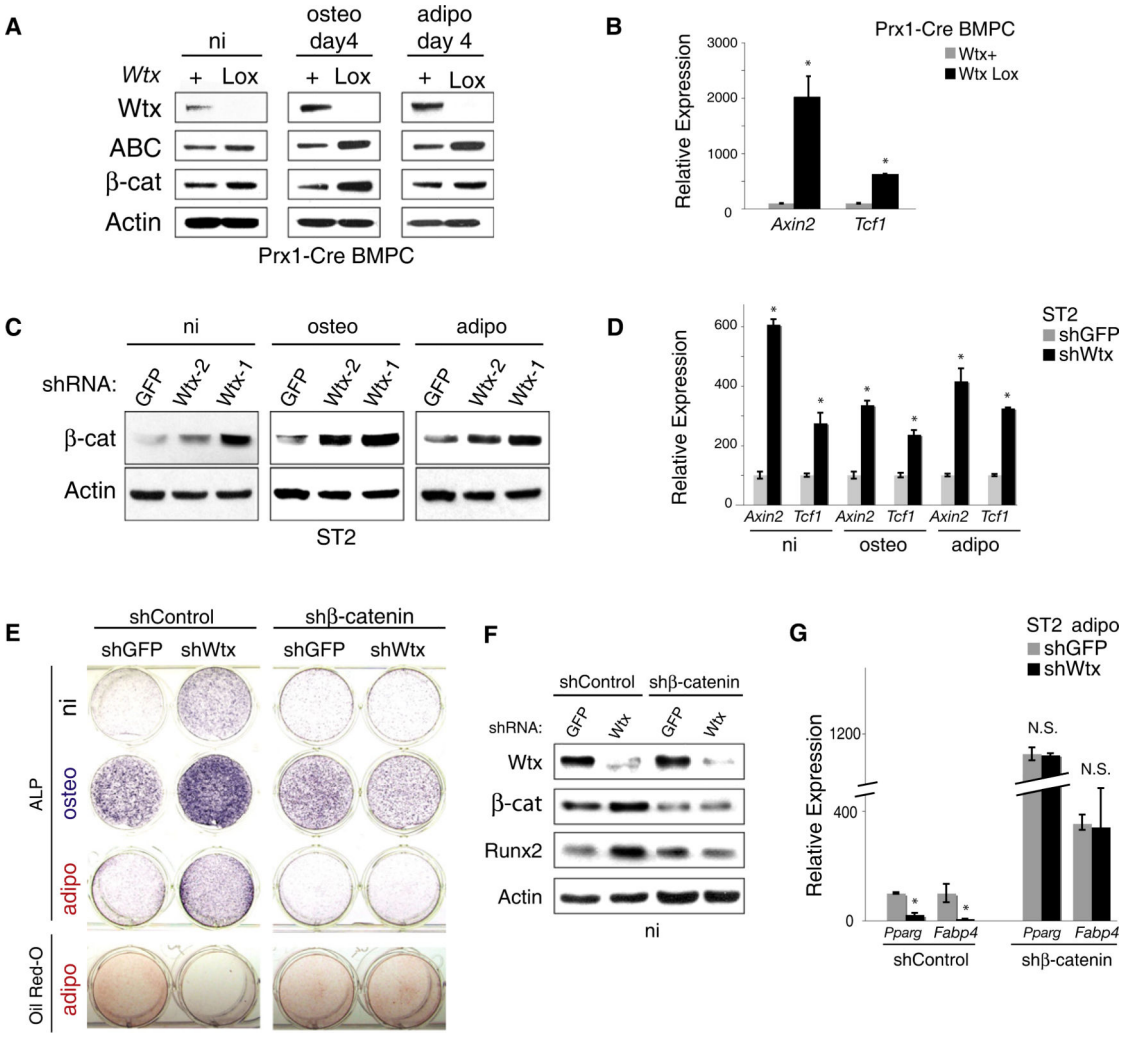

Figure 5. Wtx-Mediated Control of β-Catenin Levels in BMPCs Determines Osteoblast and Adipocyte Specification

(A and B) *Prx1-Cre;Wtx*$^{+/Y}$ and *Prx1-Cre;Wtx*$^{lox/Y}$ BMPCs were grown under the indicated conditions for 4 days and analyzed for expression of Wtx, active β-catenin (ABC), and total β-catenin (β-cat) by western blot (A) and the β-catenin target genes, *Axin2* and *Tcf1*, by qRT-PCR (B).

(C and D) ST2 cells expressing *shGFP* or different shRNAs targeting *Wtx* (*Wtx-1* and *Wtx-2*) were grown under the indicated conditions for 4 days and analyzed for expression of total β-catenin by western blot (C) and *Axin2* and *Tcf1* by qRT-PCR (D).

(E–G) ST2 cells expressing *shGFP* or *shWtx* in combination with *shControl* or *sh-β-catenin* were grown under noninducing (ni) and osteogenic (osteo) conditions for six days or in adipogenic (adipo) conditions for 12 days and analyzed for ALP and oil red O staining (E); Wtx, β-catenin, and Runx2 expression by western blot (F); and expression of *Pparg* and *Fabp4* by qRT-PCR (G). *β-catenin* knockdown rescues both the increased in ALP staining and reduction in oil red O staining caused by *Wtx* knockdown, and also restores normal *Runx2* and *Pparg* expression. See also Figure S7.

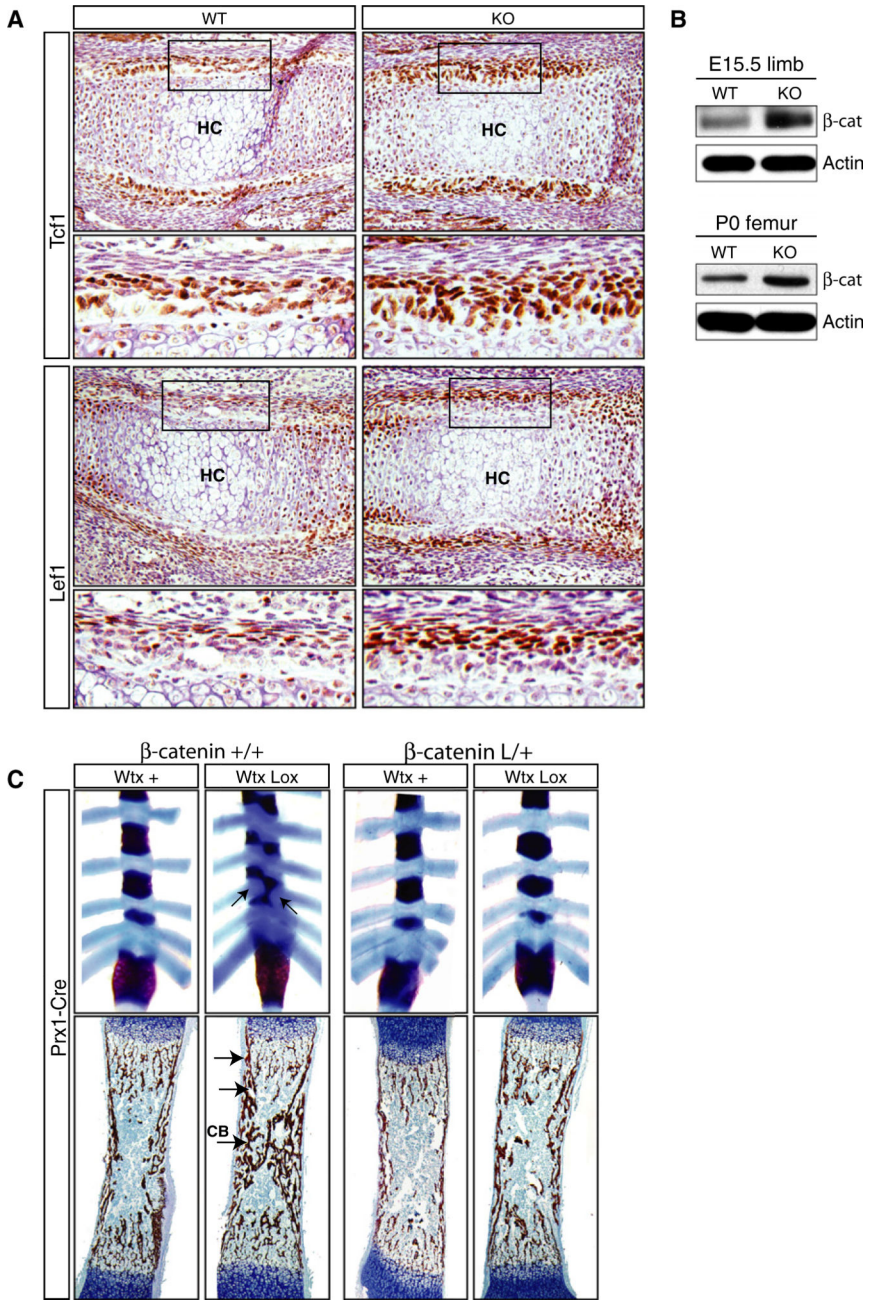

Figure 6. Wtx Modulates β-Catenin Activity during Bone Development

(A) IHC for Tcf1 and Lef1 in E14.5 wild-type and *Wtx* null humerus. HC, hypertrophic chondrocytes.

(B) Western blot analysis for total *β-catenin* protein levels in wild-type and *Wtx* null limbs at E15.5 and time of birth.

(C) Mice with the *Prx1-Cre*, Wtx^{lox}, and $\beta\text{-}catenin^{lox}$ alleles were crossed to generate compound mutants with the indicated genotypes. Skeleton preparation (top) and Von Kossa staining (bottom) of neonates show, respectively, that dysplasia of the sternum and accumulation of femoral cortical bone (CB) in *Prx1-Cre;* Wtx^{lox} mice is suppressed by concurrent *β-catenin* hemizygosity. See also Figure S7.

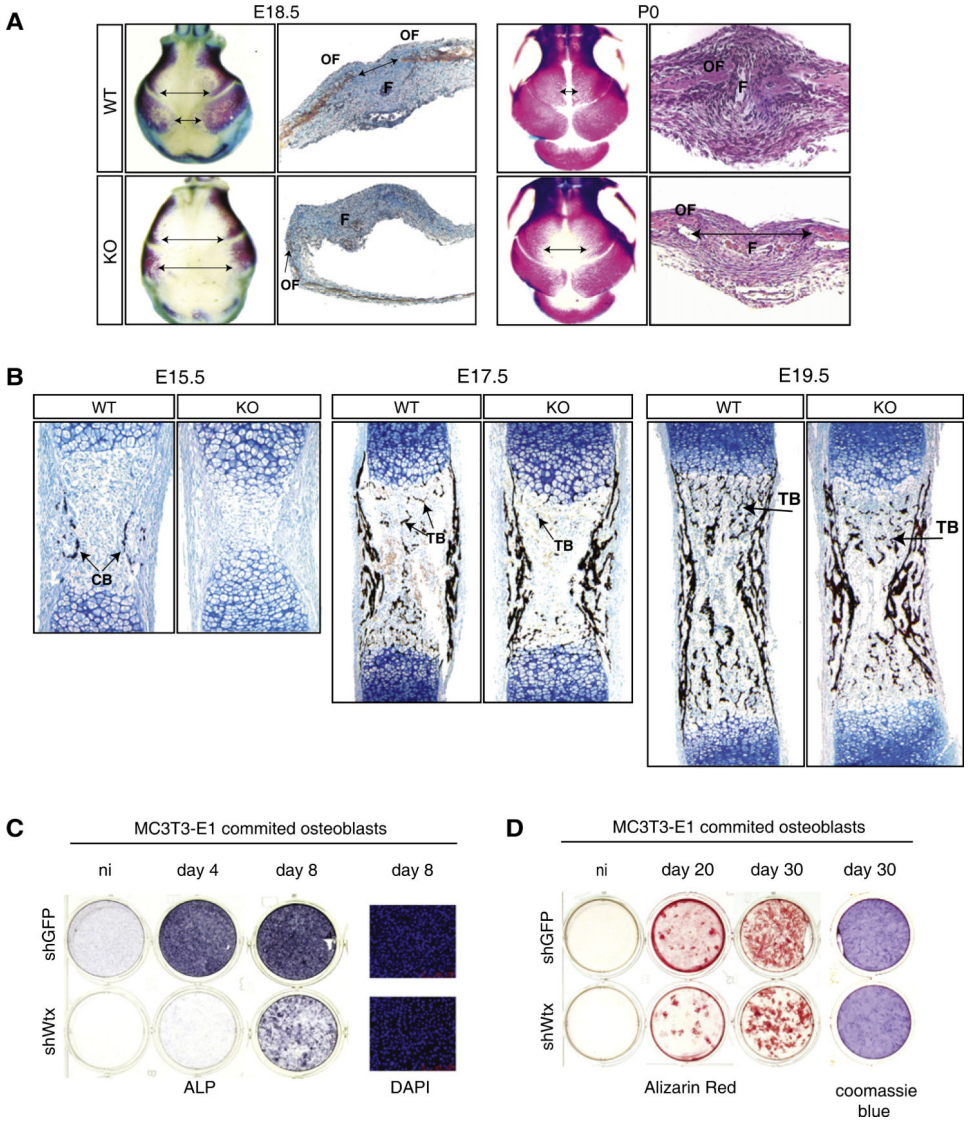

Figure 7. *Wtx* Inactivation Impairs Maturation of Committed Osteoblasts

(A and B) Delayed ossification in *Wtx* null embryos. *Wtx* null embryos (E18.5) and neonates (P0) were characterized by wide cranial fontanelles (F) as revealed by skeleton preparation (A, first and third columns), Von Kossa staining (second column), and H&E staining (fourth column). OF, ossification front. Staining of femurs with Von Kossa showing that *Wtx*-deficient mice have delayed mineralization of cortical bone (CB) at E15.5 and reduced formation of trabecular bone (TB) at E17.5 and E19.5 (B).

(C and D) *Wtx* knockdown impairs osteoblast differentiation of MC3T3 pre-osteoblasts as determined by ALP staining (C) and Alizarin red staining (D) at the indicated time points. DAPI (C) and Coomassie blue staining (D) indicate that the total number of cells were unaffected. See also Figure S8.

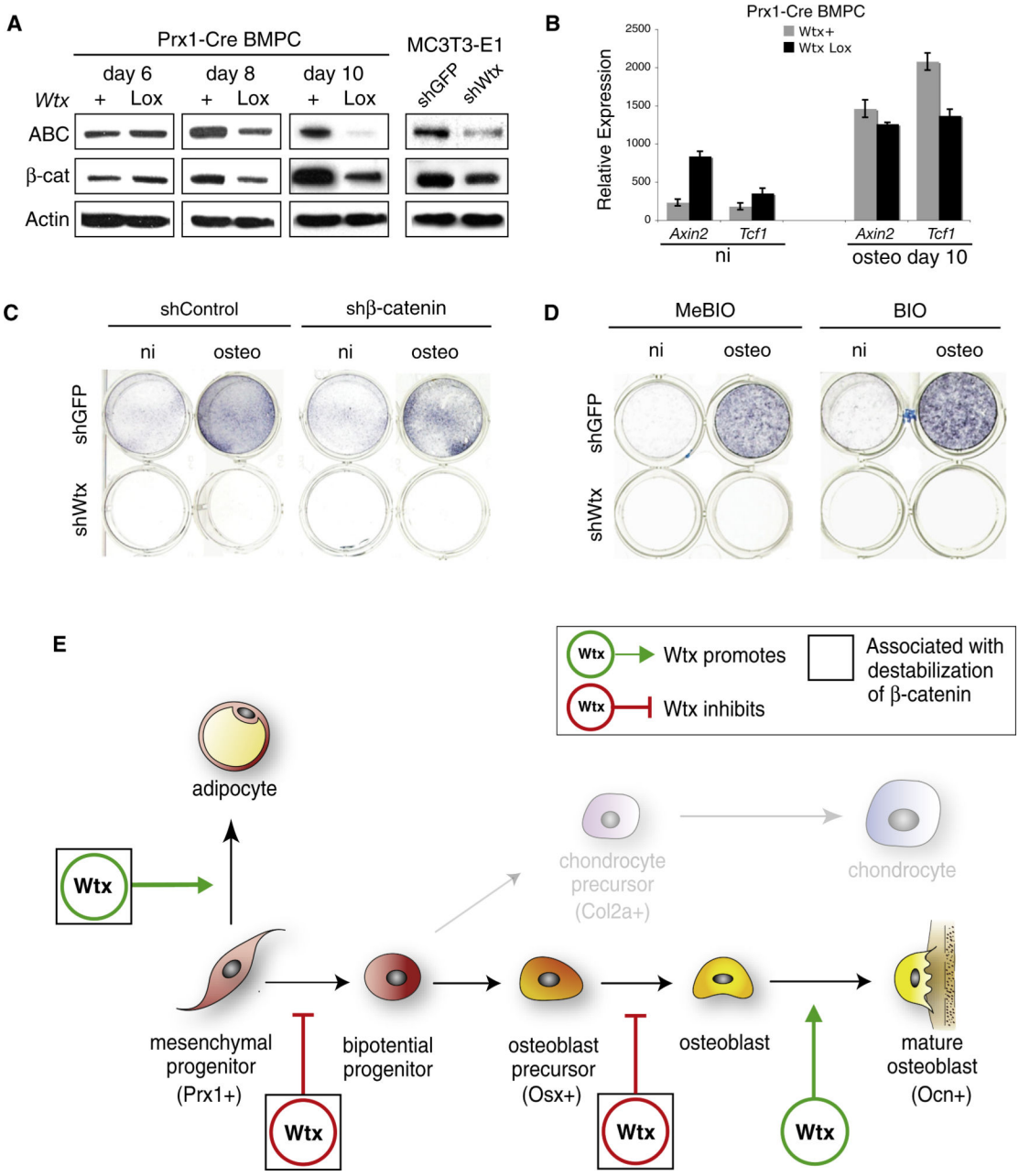

Figure 8. Wtx Inactivation Impairs Osteoblast Maturation Independent of β-Catenin Deregulation

(A) *Wtx* inactivation in committed osteoblasts is associated with reduction in activated β-catenin (ABC) and total β-catenin (β-cat) as shown in the *Prx-Cre* BMPCs and MC3T3-E1 models at the indicated time points.

(B) Expression of β-catenin target genes in *Prx1-Cre;Wtx*$^{lox/+}$ and control BMPCs. Cells were noninduced (ni) or grown 10 days under osteogenic (osteo) conditions.

(C and D) ALP staining of MC3T3-E1 cells grown under noninducing (ni) or osteogenic conditions (osteo) for 6 days and expressing sh*β-catenin* and sh*Wtx* singly or in combination shows that *β-catenin* knockdown fails to rescue the loss of ALP staining caused by *Wtx*

inactivation (C). BIO enhances ALP staining in control *shGFP*-expressing cells but fails to rescue the defective ALP staining of *Wtx*-knockdown cells (D). MeBIO is an inert control compound.

(E) Model of Wtx function. In MPCs, Wtx decreases β-catenin levels thereby calibrating lineage commitment decisions, ensuring the appropriate balance between osteoblastogenic and adipogenic determination. Wtx also inhibits β-catenin stability in Osx^{+} osteoblast precursors, thereby restraining the osteoblastic lineage expansion. Subsequently, Wtx has a distinct function directing the terminal differentiation of committed osteoblasts, a role not associated with inhibition of canonical Wnt/β-catenin signaling.